Applied Catalysis B: Environmental 119–120 (2012) 321–328

Contents lists available at SciVerse ScienceDirect

Applied Catalysis B: Environmental

journal homepage: www.elsevier.com/locate/apcatb

Enhanced hydrothermal stability of high performance lean fuel combustion alumina-supported palladium catalyst modified by nickel

Ying Liu[a,b], Sheng Wang[a], Tianjun Sun[a], Diannan Gao[a], Chunxi Zhang[a], Shudong Wang[a,*]

[a] Dalian Institute of Chemical Physics, Chinese Academy of Sciences, Dalian 116023, Liaoning, China
[b] Graduate School of Chinese Academy of Sciences, Beijing 100039, China

ARTICLE INFO

Article history:
Received 6 December 2011
Received in revised form 10 February 2012
Accepted 28 February 2012
Available online 15 March 2012

Keywords:
Ventilation air methane combustion
Palladium
$NiAl_2O_4$ spinel
Lattice mismatch

ABSTRACT

The hydrothermal stability of Pd-based methane combustion catalyst was investigated under lean-fuel conditions, such as ventilation air methane. For the catalyst, the active component Pd was impregnated on Ni-modified alumina supports which were prepared by a modified method. The method was coupled with the conventional co-precipitation and hydrothermal synthesis process. A series of Pd catalysts and supports prepared, which had the Ni/Al ratios of 1:4, 1:2 and 1:1, were characterized by BET, CO-chemisorption, XRD, TPR, SEM and TEM. The relationship between active sites and supports was studied using HRTEM. In addition, the performances for lean methane combustion of all catalysts were studied. Results showed that the catalyst on well crystallized $NiAl_2O_4$ spinel support exhibited the superior hydrothermal stability. Methane conversion remained 96% after 3200 h at 873 K. Such excellent catalytic performance has been validated to relate to the stabilizing effect of support and the least lattice mismatch between $NiAl_2O_4$ and Pd, which contributed to high Pd dispersion.

1. Introduction

Coal mine methane is not only a greenhouse gas but also a wasted energy resource if not utilized correctly [1–4]. It is well known that methane is the second largest contributor to global warming after carbon dioxide, and it has a global warming potential 21 times that of carbon dioxide [5]. Approximately 70% of all coal mining related emissions are from mine ventilation air, and large amounts of methane are discharged into the atmosphere with it. Therefore, the clean utilization of ventilation air methane (VAM) is an important issue for environmental sustainability and for the increase of energy efficiency. However, VAM emitted from most mines contains very low concentrations of methane (0.1–1.0 vol.%), which determines it is a difficult source of methane to use. Accordingly, most work has focused on the oxidation of very low concentration methane. These processes may be classified into thermal oxidation and catalytic oxidation in terms of the combustion kinetic mechanisms [1]. As compared with thermal oxidation, catalytic oxidation is advantageous because it can minimize the formation of NO_X [6].

Catalytic combustion of lean methane has been extensively investigated during the last decades [1,2,5,7–9]. The low concentration of methane [1,3] and a negative effect of water [10–18] are two major problems on the combustion reaction in mine ventilation air. On one hand, the volume of ventilation air is large and the methane resource is diluted in concentration. On the other hand, it has been found that water is absorbed or even it reacts with active sites to form inactive hydroxyl groups on the catalyst surface, therefore blocking the active sites [10–12]. The reaction is approximately negative first order in water concentration [11,13,19]. Burch et al. [20] proposed that the decomposition of palladium hydroxide and breaking the OH bond in the hydroxide were the rate-limiting step for methane oxidation. Consequently, the application of catalytic combustion for the ventilation air methane requires an acceptable activity of the catalyst even in the reaction mixture with high concentration of steam. Up to now, to solve the hydrothermal stability of catalyst still be the technical bottleneck of mitigation and utilization of VAM. There is a lack of hydrothermal stability data on catalytic combustion of lean methane, and the longest reaction time data was reported by Yamamoto and Uchida [21], in which after 2500 h the activity was about 50%.

It is well known that the support plays an important part in determining the activity and long-period stability of the catalyst [22]. Suitable support has to be resistant to the high temperature application and it has to maintain the metal dispersion of the catalyst during operation. Among many catalysts, the alumina-supported palladium catalysts are renowned for their high activity in methane combustion under lean-burn conditions [23–25]. However, the thermal stability of the catalyst is a limiting factor in this application, especially when additional water vapor is included in

* Corresponding author. Tel.: +86 411 84662365; fax: +86 411 84662365.
E-mail address: wangsd@dicp.ac.cn (S. Wang).

0926-3373/$ – see front matter © 2012 Elsevier B.V. All rights reserved.
doi:10.1016/j.apcatb.2012.02.032

the feed stream [12–14,26,27]. The addition of promoters such as metal oxide to alumina-supported palladium catalysts could be useful to enhance both catalytic activity and stability. Several studies [7,17,28–39] have investigated the catalytic activities of alumina supported palladium catalysts modified by oxide additives, such as α-Al_2O_3, $Ce_xZr_{1-x}O_2$, Ni, Co, La, and Mg, which can enhance the activity and stability of catalyst. However, the problem of inhibition by water in the feed stream has not been solved, and little detailed study has been focused on the relationship between active sites and supports.

With the aim of developing high performance catalyst for oxidation of VAM and other lean fuel methane, this paper introduces an innovative preparation process to produce a hydrothermal stable Al_2O_3-based palladium catalyst promoted with Ni element, in which the hydrothermal stability of a desired catalyst was performed under the given conditions over 3000 h. The effect of adding Ni to the Al_2O_3 support and the interaction between active phase and support are also discussed. The results are interpreted on the basis of the structural and morphological properties determined by BET, CO-chemisorption, XRD, TPR, SEM, TEM and HRTEM characterizations.

2. Experimental

2.1. Catalyst preparation

The NiO–Al_2O_3 composite supports were prepared via a modified conventional method combined with co-precipitation and hydrothermal synthesis process, initialized with mixing aqueous solutions of $Ni(NO_3)_2$ and $Al(NO_3)_3$. The mixed solutions of aluminum nitrate (0.2, 0.4 and 0.8 mol L^{-1}, respectively) and nickel nitrate (0.2 mol L^{-1}), which were prepared dissolving $Al(NO_3)_3{\cdot}9H_2O$ and $Ni(NO_3)_2{\cdot}6H_2O$ in deionized water, was stirred for 15 min, and then was slowly added to an excess of $NaHCO_3$ aqueous solution with vigorous stirring. The final pH value of the mixed solution was 8. The addition of the base induced the precipitation of a gelatinous solid with light yellowish green color. Subsequently, the mixture was transferred into a Teflon autoclave after stirred for 30 min in a glass reactor. The Teflon autoclave was sealed in a stainless steel vessel and maintained at 423 K for 5 h; afterwards, the mixture was cooled and the target precipitate was filtered and washed repeatedly with deionized water. The obtained precipitate was dried at 353 K for 10 h and calcined in air at 673 K for 2 h. Based on the processes above, the mixed oxides NiO–Al_2O_3 with Ni/Al ratios of 1:4, 1:2 and 1:1 were prepared, respectively. The as-synthesized sample was smashed and grinded into 120 mesh powders, then was punched into 15 mm tablets with 2% graphite and crushed to 16–24 mesh. The pellets were finally calcined at 1373 K for 2 h. These supports are designated as "as-prepared" supports.

Supported Pd catalysts were prepared by the incipient wetness impregnation method using an aqueous solution of $PdCl_2$. As-prepared NiO–Al_2O_3 mixture was added into the solution under ultrasonic concussion. After impregnation, the samples were dried under vacuum overnight at 393 K and calcined in air at 473 K for 2 h. After washed several times with deionized water, the Pd loading was about 0.6 wt.%. These catalysts are indicated as "as-prepared" catalysts.

The samples were denoted as Pd/NiO–$2Al_2O_3$, Pd/NiO–Al_2O_3 and Pd/2NiO–Al_2O_3 for the supports with Ni/Al ratios of 1:4, 1:2 and 1:1, respectively.

2.2. Characterization

Surface areas of the as-prepared samples were characterized according to the BET method by nitrogen adsorption at the liquid N_2 temperature in a Quantachrome NOVA2200e instrument. Prior to analysis, the samples were degassed under vacuum at 573 K for at least 2 h. The pore size distribution and total pore volume were determined by using the BJH (desorption) method.

The dispersion of palladium was measured through CO-chemisorption experiments on a Quantachrome CHEMBET Pulsar adsorption instrument. Before analysis, the catalyst was reduced in H_2/N_2 at 523 K for 4 h. The adsorption measurements were performed at 298 K in a flow of He. The dispersion of palladium was calculated from the total CO uptake by assuming a stoichiometry of CO/Pd = 1.

The X-ray diffraction (XRD) measurements were carried out on a Rigaku RINT D/MAX-2500/PC diffractometer with Cu Kα radiation at 200 mA and 40 kV. The operating parameters were 2 theta range scanning from 10 to 80°, scan step size of 0.02° and scan rate of 5°/min. The as-prepared catalyst powders were analyzed without further treatment and the phase identification was carried out using the reference JCPD database.

The temperature programmed reduction (TPR) experiments were performed on a flow system at a Quantachrome CHEMBET 3000 adsorption instrument equipped with a TCD detector. A water trap removed moisture from the TPR effluent stream before the TCD. Prior to reduction, 150 mg of the as-prepared catalyst was placed into a quartz reactor and dried in an argon flow at 473 K for 1 h. Then the sample was reduced in a 5% H_2/Ar (30 mL min^{-1}) flow system at a rate of 5 K min^{-1} from 373 to 1193 K.

The scanning electron microscopy (SEM) analysis was obtained with an FEI Quanta 200F equipment. The reduced catalysts (10% H_2/N_2 at 723 K for 2 h) were stuck on the 1 cm diameter holders by using double-faced adhesive tape.

The transmission electron microscopy (TEM) measurement was carried out with an FEI Tecnai G^2 Spirit equipment operated at an accelerating voltage of 120 kV. The reduced catalyst powder was ultrasonically dispersed in ethanol and dropped onto a copper grid with amorphous carbon film, then dried in air.

The high resolution transmission electron microscopy (HRTEM) measurement was made with an FEI Tecnai G^2 F30 S-Twin equipment at an accelerating voltage of 300 kV. The energy dispersive X-ray spectroscopy (EDS) was used in scanning transmission electron microscope (STEM) mode. The reduced catalyst powder was ultrasonically dispersed in ethanol and dropped onto a copper grid with amorphous carbon film, then dried in air.

2.3. Catalytic evaluation

The hydrothermal stability of catalysts was tested in a fixed-bed tubular reactor at atmospheric pressure. The quartz reactor (8 mm i.d.) packed with 1.0 g catalyst was put into the tubular oven controlled by a PID temperature regulator. The feed gas containing 0.4 vol.% of CH_4, 4 vol.% of H_2O and balancing air was supplied to the catalyst bed through a mass flow controller at a gas hourly space velocity (GHSV) of 80,000 h^{-1} and the temperature was maintained at 873 K. The selection of 4 vol.% of H_2O was based on the actual water content of VAM. The compositions of the feed gas and the combustion flue gas were analyzed by an on-line gas chromatograph with an FID detector. Prior to each run, the catalyst was reduced in 10% H_2/N_2 at 723 K for 2 h.

3. Results

3.1. Supports

The durability test was performed with GHSV of 80,000 h^{-1} and an inlet gas temperature of 873 K. The observed products were carbon dioxide and water, indicating complete combustion occurred

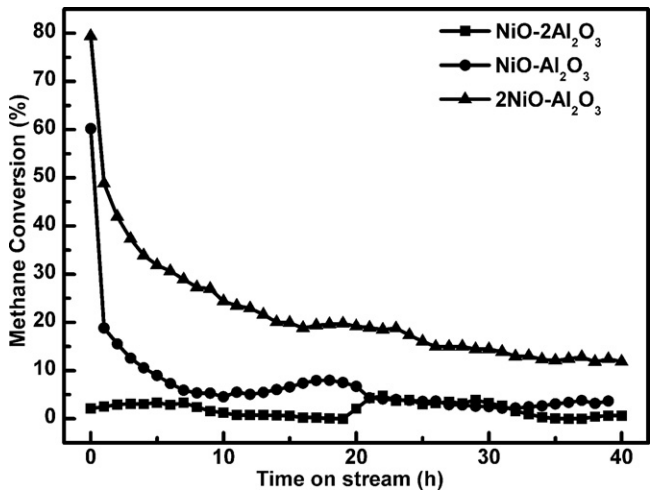

Fig. 1. Methane conversion versus time on stream over different supports in the presence of 40,000 ppm of water. Reaction conditions: CH_4: 0.4 vol.%, air as balance. GHSV = 80,000 h^{-1}, reaction temperature = 873 K.

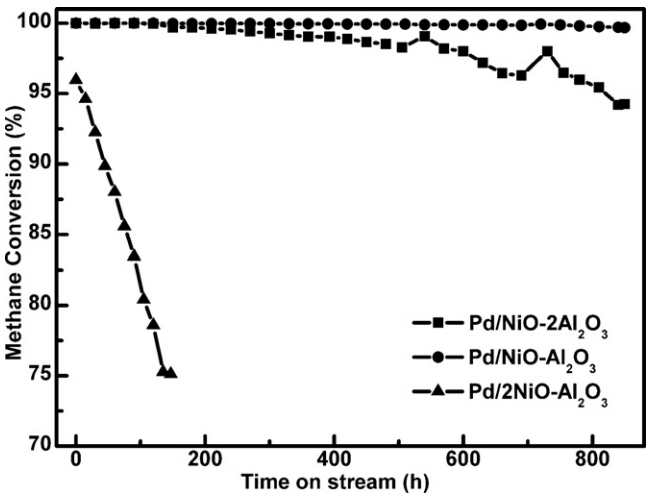

Fig. 2. Methane conversion versus time on stream over different catalysts in the presence of 40,000 ppm of water. Reaction conditions: CH_4: 0.4 vol.%, air as balance. GHSV = 80,000 h^{-1}, reaction temperature = 873 K.

in the reaction. Fig. 1 shows the conversion-versus-time on stream of three as-prepared supports. The catalytic durability of supports increased continuously with the nickel content. Though the supports NiO–Al_2O_3 and 2NiO–Al_2O_3 initially had slight activities, the methane conversions decreased sharply and then stabilized at a considerably lower conversion for the rest of the test period. The conversions were only 4% and 12% after 40 h on stream, respectively. NiO–$2Al_2O_3$ had a different combustion profile from the others, even with little activity detected during reaction, which was the lowest conversion of CH_4 among the above-mentioned supports.

Textural data, including the BET surface area, pore volume and pore diameter of as-prepared and spent supports are collected in Table 1. Compared to the Al_2O_3 prepared by the same method (S_{BET} = 38 m^2 g^{-1}), the specific surface areas of the supports were decreased with the addition of Ni. In addition, the specific surface areas shifted toward a lower one concomitantly with the increase of Ni loading, however, the activity of supports increased. The reaction at 873 K for 40 h led to a slight decrease in the surface area, especially for 2NiO–Al_2O_3. In addition, different from the other two supports, 2NiO–Al_2O_3 sample possessed visibly smaller pore volume and pore diameter.

3.2. Methane combustion of catalyst

As illustrated in Fig. 2, the hydrothermal stability of the supported Pd catalyst was strongly dependent on the Ni content, though high initial methane conversion was observed for each catalyst. It should be noted that Pd/NiO–Al_2O_3 catalyst gave the CH_4 conversion of 99.6% without any loss in catalytic activity during 850 h running. The CH_4 conversion over Pd/NiO–$2Al_2O_3$ was stable during the first 200 h and then showed a small drop, with a final conversion around 94% after 850 h. It is assumed that the deactivation will further increase. However, the Pd/2NiO–Al_2O_3 catalyst was quite active initially, but the activity dropped severely during the course of the experiment. The CH_4 conversion nearly decreased by 18% just less than 150 h, even though the temperature and the other reaction parameters were kept constant. Thus, Pd/NiO–Al_2O_3 had the highest catalytic durability among the three catalysts.

Later the long duration test was carried out over Pd/NiO–Al_2O_3 catalyst. As shown in Fig. 3, the methane conversion for Pd/NiO–Al_2O_3 remained at about 96% after a 3200 h test at 873 K, indicating the catalytic activity of this catalyst decreased very slightly. Therefore, it seems that this catalyst is the appropriate candidate for lean methane combustion because of its superior hydrothermal stability.

Table 1
BET surface area, pore volume and pore diameter of supports, before and after reaction.

Support	Surface area/m^2 g^{-1}		Pore volume/cm^3 g^{-1}		Pore diameter/nm	
	As-prepared	Spent	As-prepared	Spent	As-prepared	Spent
NiO–$2Al_2O_3$	32	31	0.18	0.15	18.2	18.1
NiO–Al_2O_3	22	20	0.14	0.13	18.0	18.2
2NiO–Al_2O_3	13	9	0.06	0.04	3.8	3.7

3.3. Characterization of catalyst

There were no significant differences on textural data between supports and catalysts due to low Pd loading. The differences in the catalytic stability of catalysts (Pd/NiO–Al_2O_3 > Pd/NiO–$2Al_2O_3$ > Pd/2NiO–Al_2O_3) likewise could not be explained directly by the differences in the surface area. The large surface area plays an important role in promoting the

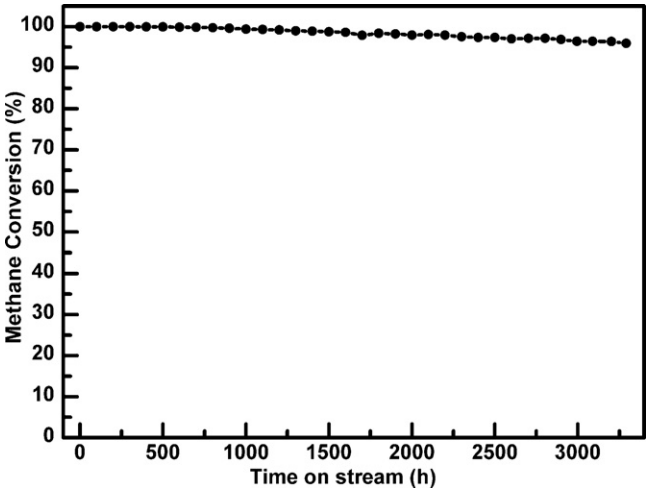

Fig. 3. Methane conversion versus time on stream over Pd/NiO–Al_2O_3 catalyst in the presence of 40,000 ppm of water. Reaction conditions: CH_4: 0.4 vol.%, air as balance. GHSV = 80,000 h^{-1}, reaction temperature = 873 K.

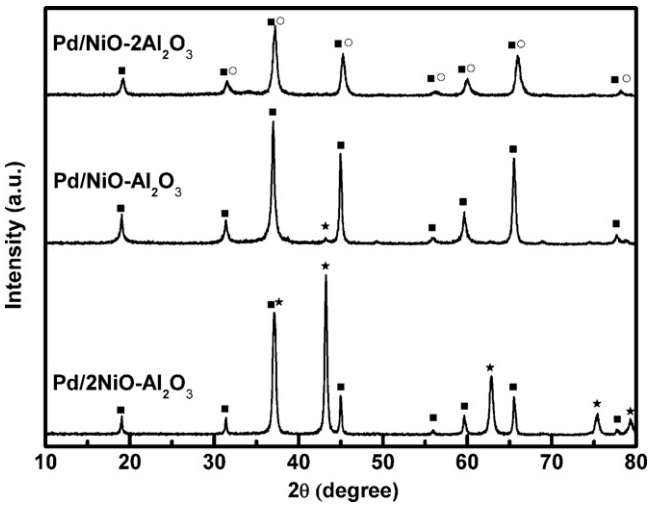

Fig. 4. XRD patterns of $Pd/NiO–2Al_2O_3$, $Pd/NiO–Al_2O_3$ and $Pd/2NiO–Al_2O_3$ catalysts. Where ■, $NiAl_2O_4$; ○, σ-Al_2O_3; □, NiO.

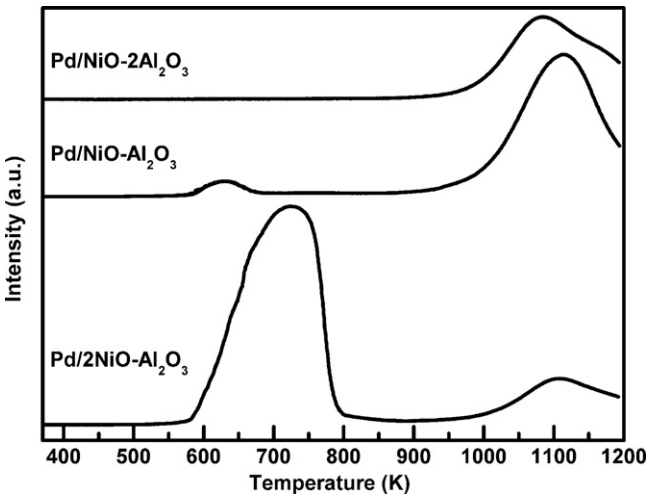

Fig. 5. H_2-TPR profiles of $Pd/NiO–2Al_2O_3$, $Pd/NiO–Al_2O_3$ and $Pd/2NiO–Al_2O_3$ catalysts.

overall capability of catalyst, but it is not applicable in the present samples, being consistent with results reported in many studies [30,34,40,41]. A significant variation of Pd dispersion values, calculated by CO-chemisorption analysis, could be observed for three catalysts. Pd on the $NiO–Al_2O_3$ support shows a higher dispersion value (14.9%) than on the $NiO–2Al_2O_3$ and $2NiO–Al_2O_3$ supports (7.7% and 2.8%, respectively).

The XRD patterns of catalysts are shown in Fig. 4. Unfortunately, neither palladium nor palladium oxide was detected in all of the samples. This is in agreement with the results found by Lapisardi et al. [42] and Maione et al. [43], in the case of Pd-based catalysts characterized by a Pd loading lower than 2%. Nevertheless, XRD analysis provided valuable information about the nature of different phases present in the catalysts.

The $NiAl_2O_4$ phase, formed by the interaction between nickel oxide and alumina during the calcination at high temperature, could be observed in all the catalysts, which was confirmed by the peaks appearing at 37.0, 45.0 and 65.5° related to the reflection planes (3 1 1), (4 0 0) and (4 4 0) of $NiAl_2O_4$, respectively. Since the 2θ values of $NiAl_2O_4$ and σ-Al_2O_3 are so close, only overlapped but broadened peaks were obtained in $Pd/NiO–2Al_2O_3$. Concerning $Pd/NiO–Al_2O_3$ sample, the diffraction peaks of $NiAl_2O_4$ were clearly identified and became sharper, indicating well formation of spinels. On the other hand, a very weak peak for NiO was observed. It has been reported that stoichiometric $NiAl_2O_4$ seemed difficult to be prepared as pure phase and formed easily small zones of free nickel oxide [44]. In the case of $Pd/2NiO–Al_2O_3$ sample, besides $NiAl_2O_4$ spinel, the diffraction analysis also indicated the formation of NiO which was identified by the presence of the peaks appearing at 2θ equal to 37.2, 43.3 and 62.8° related to the reflection planes (1 1 1), (2 0 0) and (2 2 0) of NiO, respectively. The crystal particle size for NiO was about 25 nm as determined by Scherrer's formula.

The temperature programmed reduction (TPR) with hydrogen of catalysts is shown in Fig. 5. Since the palladium oxides are easily reduced below 373 K, the reduced peaks observed in TPR mainly originated from the oxygen species in the supports. The fact that all the samples presenting peaks at 1083–1113 K due to the stoichiometric spinel $NiAl_2O_4$ was proposed in the literature [44,45]. For $Pd/NiO–2Al_2O_3$, the addition of excessive Al led to the formation of Al_2O_3–$NiAl_2O_4$ solid solution. Thus, the reduction peak of $Pd/NiO–2Al_2O_3$ was also weakened.

$Pd/2NiO–Al_2O_3$ samples show a strong and broad reduction peak from 580 K to 800 K, assigned to free NiO. For $Pd/NiO–Al_2O_3$, a weak reduction peak also appeared within this temperature range, attributing to a small amount of NiO not converted into $NiAl_2O_4$. In fact, free NiO was also detected by XRD spectrum (Fig. 4). The reduction of $Pd/NiO–Al_2O_3$ occurred at lower temperatures compared to that of $Pd/2NiO–Al_2O_3$ while the reduction peak maximum of $Pd/2NiO–Al_2O_3$ appeared fairly close to that of bulk NiO. It is the reason that the higher NiO content led to larger particle size and higher reduction temperature [46].

The scanning electron microscopy (SEM) was used to observe a possible morphological change in $Pd/NiO–2Al_2O_3$, $Pd/NiO–Al_2O_3$ and $Pd/2NiO–Al_2O_3$ catalysts after the long duration tests. The reduced catalysts, before the reaction treatment, are referred as "fresh" catalysts. Fig. 6(a) and (b) reveals the presence of small grains on the surface of the $Pd/NiO–2Al_2O_3$ catalyst, which should be palladium particles. The particles in Fig. 6(b) seem to be more and bigger than the ones in Fig. 6(a); and it displays that the palladium particle size increased after the long-period test. As can be seen in Fig. 6(c) and (d), the support shows a compact structure, and palladium particles were not observed for both fresh and spent catalysts. Furthermore, no significant morphological change occurred on the surface of catalyst during the catalytic test. Fig. 6(e) and (f) shows the SEM pictures of $Pd/2NiO–Al_2O_3$ catalyst before and after the long duration test. Particles of nearly spherical shapes (10–40 nm) were presented on fresh and spent catalysts. According to the XRD phase analysis data (Fig. 4), $Pd/2NiO–Al_2O_3$ sample consisted of NiO with an average crystallite size of 28 nm, which was consistent with the particle size observed in Fig. 6(e) and (f). In contrast, palladium particles cannot be confirmed on the catalyst surface owing to the influence of high concentration of Ni on the support. In conclusion, evident differences are noticed on SEM micrographs among the three samples. The morphology and microstructure of the deposited Pd strongly depend on the nature of the support.

The transmission electron microscopy (TEM) studies of the three catalysts after reduced in 10% H_2–N_2 were carried out to visually confirm various dispersion of the palladium phase, which are shown in Fig. 7(a)–(c). The catalyst was in the reduced crystalline Pd state after this pretreatment. The TEM micrographs suggest that all the catalysts contained spherical particles. As illustrated in Fig. 7(a), deposited palladium particles are located on local $NiO–2Al_2O_3$ support surface. In some regions of $NiO–2Al_2O_3$ support, Pd particles were hardly observed. For $Pd/NiO–Al_2O_3$ catalyst, homogeneous and well-defined spherical support particles of 20–70 nm in size are evidenced in Fig. 7(b). Palladium particles are visible as black dots and are rather homogeneously distributed over the supports with sizes normally in the range of 3–8 nm; for random

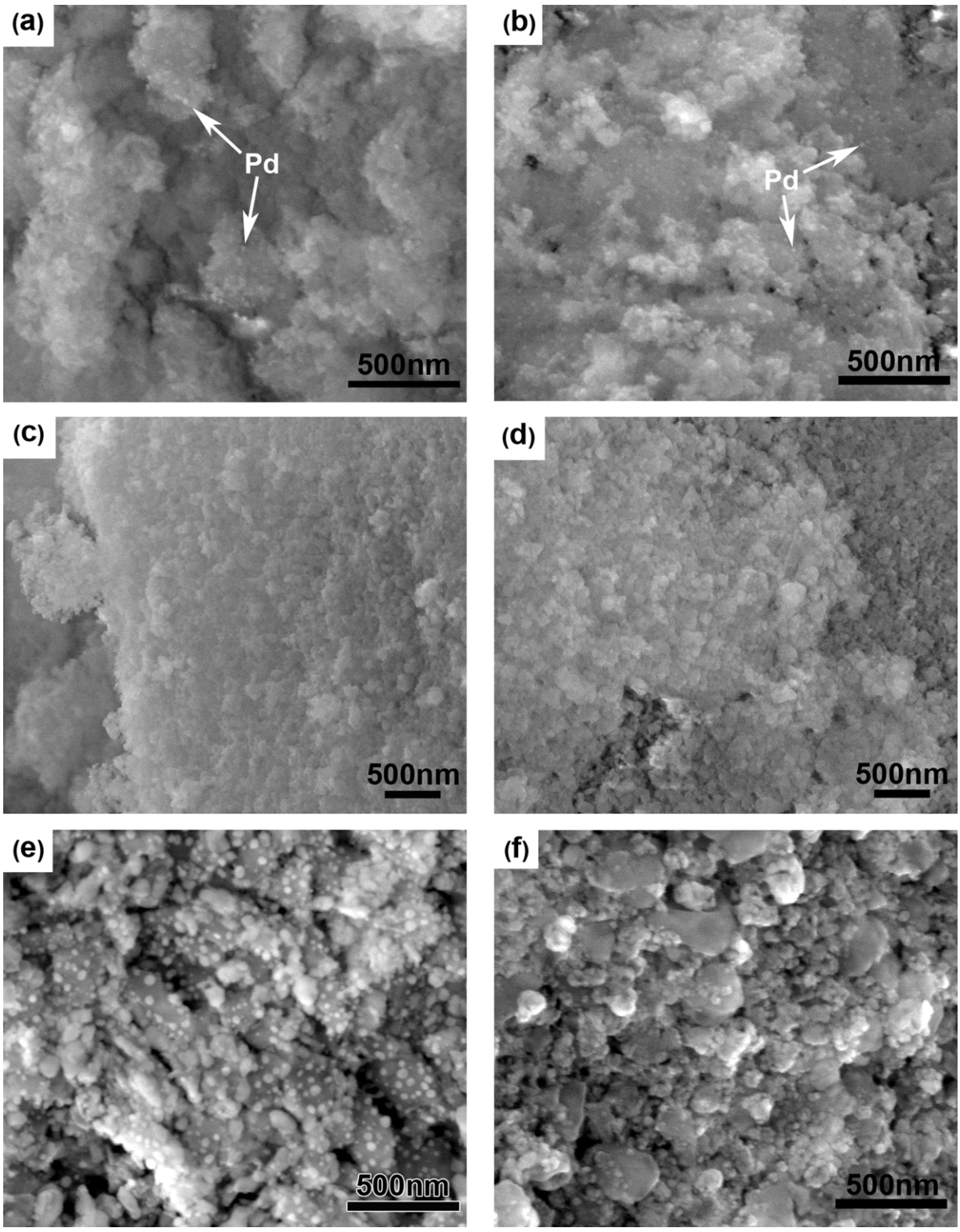

Fig. 6. SEM images of catalysts: (a) fresh Pd/NiO–2Al_2O_3 catalyst; (b) spent Pd/NiO–2Al_2O_3 catalyst; (c) fresh Pd/NiO–Al_2O_3 catalyst; (d) spent Pd/NiO–Al_2O_3 catalyst; (e) fresh Pd/2NiO–Al_2O_3 catalyst; and (f) spent Pd/2NiO–Al_2O_3 catalyst.

orientations such as this and at low magnifications the palladium particles appear approximately circular and one cannot obtain directly interpretable information about their internal or external structure. The sizes of the palladium particles were determined from numerous investigated fragments. It is worthy to note that the observed palladium particles on the NiO–Al_2O_3 support are smaller and more uniformly distributed. Fig. 7(c) shows the TEM picture of Pd/2NiO–Al_2O_3 catalyst. It displays a rather wide range of palladium particle size. Some particles (two particles seen on the right edge of the micrograph) with size around 25 nm appear to be nickel particles, which is consistent with the XRD results and SEM micrograph in Fig. 6(e). Palladium particles on supports NiO–2Al_2O_3 and 2NiO–Al_2O_3 appeared to distribute more densely than on support NiO–Al_2O_3. As a consequence, it seems that palladium particles

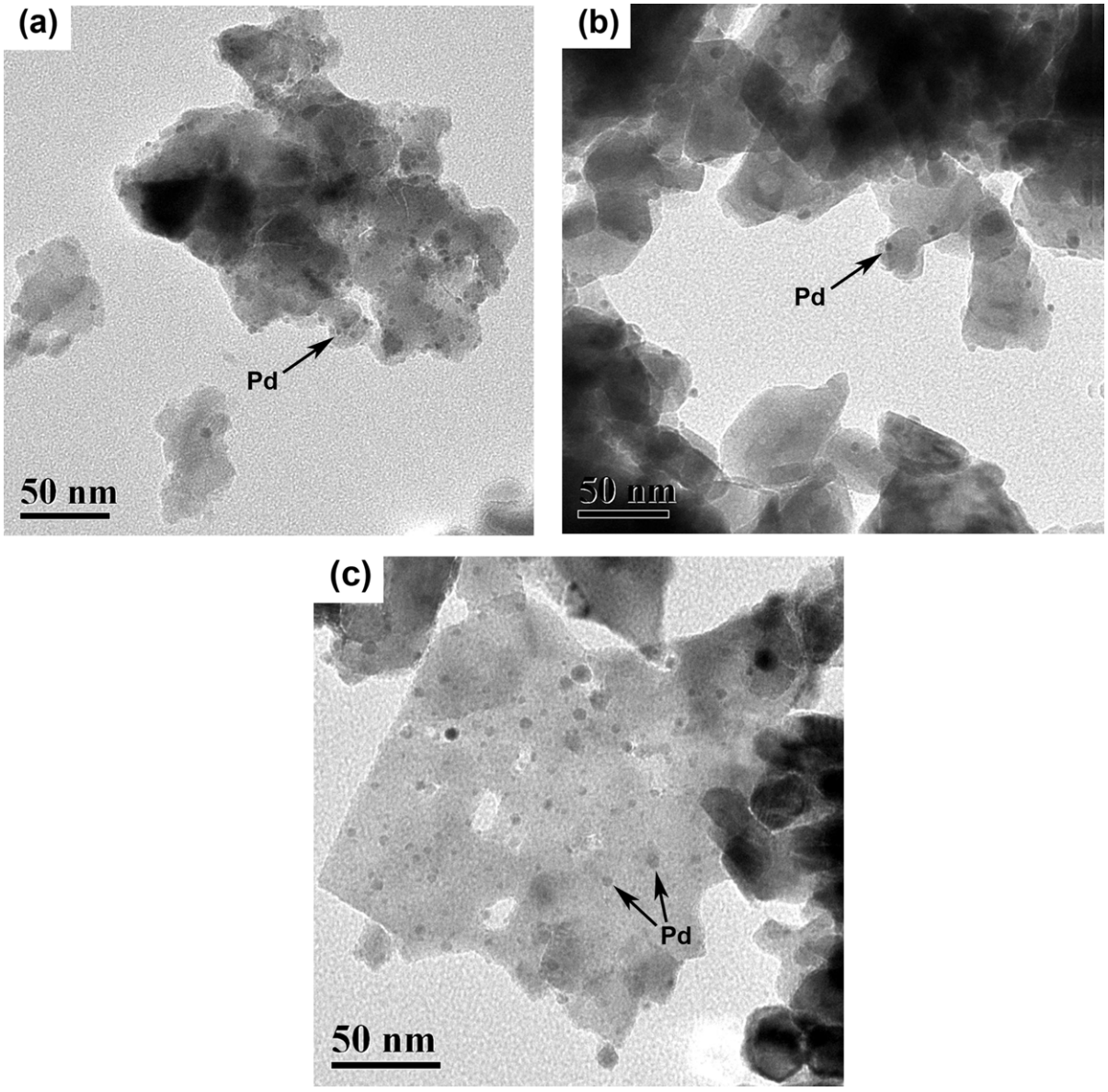

Fig. 7. TEM images of catalysts: (a) Pd/NiO–$2Al_2O_3$; (b) Pd/NiO–Al_2O_3; and (c) Pd/$2NiO–Al_2O_3$.

have higher dispersion on NiO–Al_2O_3 support, and form agglomerates more easily on NiO–$2Al_2O_3$ and $2NiO–Al_2O_3$ supports, which is in accordance with the CO-chemisorption data and SEM diagrams.

The morphology of Pd/NiO–Al_2O_3 sample was further probed with high resolution transmission electron microscopy (HRTEM). The results from EDS (data not shown) strongly suggest that Pd emission lines were present in crystal particles. All the HRTEM micrographs shown were of reduced catalysts, and therefore the particles consisting of palladium emission were in reduced state. Fig. 8 reveals that the particles distributed over the support were palladium ones, which further proved our judgment obtained above on palladium particles in the analysis of SEM and TEM diagrams. It is in accord with the TEM results that Pd metal particles smaller than 10 nm can be seen in HRTEM micrographs. The micrographs show the regular succession of the atomic planes corresponding to the different planes of the $NiAl_2O_4$ lattice. Fig. 8(a) shows the interplanar distances of $NiAl_2O_4$, 0.20 and 0.28 nm, corresponding to the $NiAl_2O_4$ (4 0 0) and (2 2 0) reflection, respectively. A representative palladium particle (within dashed) is also observed in Fig. 8(a), which presents (2 0 0) plane with an interplanar distance of 0.19 nm. Fig. 8(b) shows a hemispherical particle strongly connecting with the support. The particle presents (2 0 0) and (1 1 1) planes with interplanar distances of respectively 0.19 and 0.22 nm, characteristic of Pd. The supports present (3 1 1) and (1 1 1) planes with interplanar distances of respectively 0.24 and 0.46 nm, characteristic of the structure of $NiAl_2O_4$. A smaller contact angle of the interface also permits matching of the crystal lattices for the Pd and $NiAl_2O_4$ phase [47]. This may result in an unusual microstructure and high dispersion of palladium particle, because a strong interaction between the supported particles and the support plays a role in restraining the migration and growth of the particles.

4. Discussion

For a lean-fuel methane combustion process, the initial activities of $NiO–2Al_2O_3$, NiO–Al_2O_3 and $2NiO–Al_2O_3$ were about 2%, 60% and 80% at 873 K, respectively. And the activities will drop strongly to 1%, 4% and 12% after a 40 h run. It indicated that the activities of supports increased monotonically with the nickel content due to the

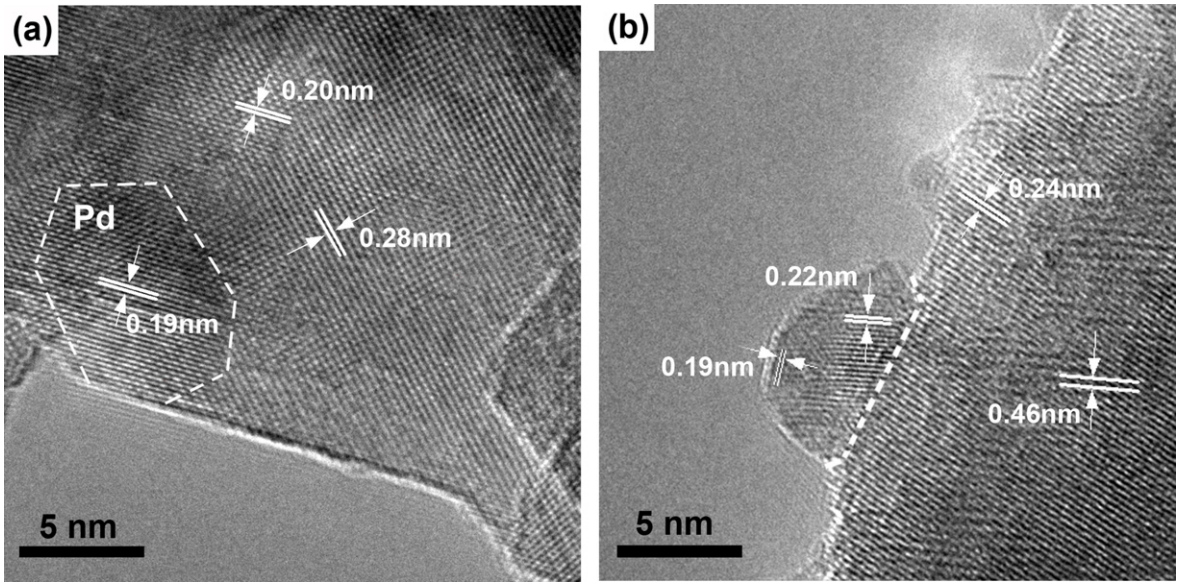

Fig. 8. HRTEM images of Pd/NiO–Al_2O_3: (a) top view of a Pd particle on support and (b) side view of Pd particles on support.

catalytic activity of NiO for methane combustion. As for NiO–Al_2O_3 support of the present study, methane should also be activated by NiO, because a small amount of NiO was not converted into $NiAl_2O_4$. The occurrence of NiO in the NiO–Al_2O_3 support was proven by XRD and TPR as above-mentioned [44]. Thus, it is easier to explain the lower activity of methane combustion for NiO–$2Al_2O_3$ support, since NiO was converted completely into $NiAl_2O_4$.

Generally, Pd based catalyst is an optimum option for the removal of CH_4 in the VAM. In our work, a part of PdO particles on supports were firstly reduced by H_2 into palladium particles at the high-temperature, thus the Pd–PdO formed on the substrate served as the active component [24,34,48]. CH_4 diffused and chemisorbed on the surface of the catalyst, whereafter it dissociated and was oxidized to CO_2 and H_2O. Normally, CH_4 prefers to combust on Pd/Al_2O_3 catalyst, and its combustion performance is considered to be dependent on the stability and activity of the catalyst [49,50].

The activity experiments of the three catalysts indicated that Pd/NiO–$2Al_2O_3$ and Pd/NiO–Al_2O_3 catalysts both had the better performance for methane combustion, especially Pd/NiO–Al_2O_3, the excellent catalytic activity and stability of which can be kept during a long period.

The activity of Pd/NiO–$2Al_2O_3$ decayed more rapidly than that of Pd/NiO–Al_2O_3, particularly after 500 h. However, with the increase of the nickel content in the support, the free NiO would increase largely, but the activity of Pd/2NiO–Al_2O_3 dropped severely. This phenomenon is unexpected in view of the other observations that the activity was enhanced with an increase of NiO content of the support and deteriorated with the increase of $NiAl_2O_4$ phase [30,40]. As shown in Figs. 2 and 4, the hydrothermal stability of the catalysts was enhanced gradually with the increase of $NiAl_2O_4$ spinel content. It has been widely demonstrated that metal–support interaction and catalyst particle morphology are interdependent parameters, which strongly influence the activity of the catalyst. Accordingly, there are two possible reasons for above experimental results: (1) the promoter NiO reacting with the support of Al_2O_3 enhanced the stability of the support, and (2) the palladium particles were locally crystallized or atomically ordered at the interfacial region with the support, which determined the stability of active site.

It is known that most aluminum spinels are thermally stable structures, much more than transition alumina from which they have been synthesized [31,51,52]. The TPR profiles also indicate that the $NiAl_2O_4$ was stable. Therefore, the Al_2O_3 supports must be stabilized by the obtained species of $NiAl_2O_4$ spinels, and the hydrothermal stability of catalysts would be improved accordingly.

The CO-chemisorption and TEM show that the dispersion of Pd was remarkably high on NiO–Al_2O_3 support, but Pd on the supports NiO–$2Al_2O_3$ and 2NiO–Al_2O_3 both had lower dispersion, especially for 2NiO–Al_2O_3. As suggested by Yang et al. [31], the support containing γ-Al_2O_3 or excessive MgO had no benefit for the dispersion of Pd, because the former will cause serious sintering of the support, and the latter should be attributed to severe deviation from ideal spinel composition. This may be the same for the support containing σ-Al_2O_3 and excessive NiO prepared above. As a result, it seems that the well crystallized $NiAl_2O_4$ spinel is preferable for higher Pd dispersion which is beneficial to the performance of catalysts according to our experimental results.

The enhanced hydrothermal stability of Ni-modified Pd/Al_2O_3 VAM combustion catalyst can also be explained by the lattice mismatch at the interface between the palladium particles and the $NiAl_2O_4$ spinel structure.

It is known that the Pd, PdO, Ni, NiO, Al_2O_3 and $NiAl_2O_4$ crystal possibly coexist in this catalyst. The Pd, Ni, NiO, and $NiAl_2O_4$ crystal could be the face-centered cubic structures, and this nanospheres or near-spherical particles mostly show an FCC structure in the form of cuboctahedrons with their surfaces bounded by a mixture of (1 1 1) and (1 0 0) [53]. The Pd (1 1 1) and Pd (1 0 0) planes can match the corresponding planes of Ni, NiO or $NiAl_2O_4$ without the angle distortion between them. It has been reported that the interface prefers to take the least lattice mismatch [54], and lattice mismatch at the interface is important in defining the structure characteristics of the crystallite. The low-indexed planes (1 1 1) and (1 0 0) at the interface of Pd nanostructures match the (1 1 1) and (1 0 0) planes of $NiAl_2O_4$ structures with a lattice mismatch as small as 3.3%. The lattice mismatches, however, are the 7% and 9% between the Pd–Ni and Pd–NiO, respectively. Thus, there is much interface strain between Pd and Ni or NiO, and it is preferred to match with $NiAl_2O_4$ to decrease the interface mismatch energy, which has been confirmed by HRTEM (Fig. 8). Certainly, Pd and $NiAl_2O_4$ not only show the least lattice mismatch in the low-indexed planes such as (1 1 1) and (1 0 0), but they also take the least lattice mismatch between other corresponding planes. On the other hand, the migration of palladium nanoparticles on the surface of $NiAl_2O_4$ will be decreased owing to the decrease of surface energy by the

relatively small lattice mismatch and the great hydrothermal stability of $NiAl_2O_4$. As discussed above, the strong metal–support interaction effect in $Pd/NiAl_2O_4$ is responsible for the high dispersion and for the sintering-resistant behavior of the catalyst. Pd active phase will remain in the suitably dispersed state on $NiAl_2O_4$, resulting in long-term catalytic stability.

When the local temperature of 723–873 K is close to the Tammann temperature of Pd (its bulk melting point is 1823 K), the fixed orientation relationship is possibly established between the single-crystal structure of the palladium particles after reduction and $NiAl_2O_4$ particles, if the palladium particles are locally atomically ordered at $NiAl_2O_4$ surface. This may be possible if there are a few atomic layers on the surface of the palladium particles tend to melt and match with lattice of $NiAl_2O_4$ crystal in this process. Such a local ordering may be appeared for only a few atomic layers in thickness, while the rest of the palladium particles are in molten state.

In a word, $NiAl_2O_4$ support attributed to a superior catalytic performance for lean methane combustion. Concretely, it is embodied that $NiAl_2O_4$ phase has the high hydrothermal stability and the dispersion of Pd active phase is enhanced by the interaction between Pd and $NiAl_2O_4$ phase.

Although the phase of $NiAl_2O_4$ in the support plays an important role to enhance the catalytic activity by maintaining the high dispersion of the palladium particles, it is likely that other chemical properties also affect the activity [34]. The full evaluation for the catalysts is planned in the near future.

5. Conclusions

A series of Al_2O_3-based palladium catalysts promoted with Ni element were prepared by an innovative preparation process for catalytic combustion of VAM. The hydrothermal stability was enhanced with an increase of Ni content of the support until the large amount of free NiO formed. Therefore, the catalyst on nearly fully crystallized $NiAl_2O_4$ spinel support demonstrated the highest hydrothermal stability. The methane conversion of $Pd/NiAl_2O_4$ was still about 96% at 873 K after 3200 h test. When $NiAl_2O_4$ was applied as a support, the support was stabilized by the spinel and the hydrothermal stability of catalyst was improved accordingly. More importantly, the least lattice mismatch at the interface between the palladium particles and the $NiAl_2O_4$ spinel structure leads to an improved cooperation between them, which was a significant reason for the high Pd dispersion, and then for superior hydrothermal stability of the catalyst. The results suggest that $Pd/NiAl_2O_4$ catalyst is an appropriate candidate for VAM and other lean fuel methane combustion because of its superior catalytic activity and hydrothermal stability.

Acknowledgement

This work was partly supported by Chinese National Science Foundation (20806079) and the National Key Foundational Research Project (973) of China (2010CB732302).

References

[1] S. Su, A. Beath, H. Guo, C. Mallett, Prog. Energy Combust. Sci. 31 (2005) 123–170.
[2] S. Su, J. Agnew, Fuel 85 (2006) 1201–1210.
[3] B. Stasinska, A. Machocki, K. Antoniak, M. Rotko, J.L. Figueiredo, F. Goncalves, Catal. Today 137 (2008) 329–334.
[4] N.M. Kinnunen, J.T. Hirvi, T. Venalainen, M. Suvanto, T.A. Pakkanen, Appl. Catal. A: Gen. 397 (2011) 54–61.
[5] R.E. Hayes, Chem. Eng. Sci. 59 (2004) 4073–4080.
[6] X.N. Guo, G.J. Zhi, X.Y. Yan, G.Q. Jin, X.Y. Guo, P. Brault, Catal. Commun. 12 (2011) 870–874.
[7] F. Arosio, S. Colussi, A. Trovarelli, G. Groppi, Appl. Catal. B: Environ. 80 (2008) 335–342.
[8] C.Q. Chen, W. Li, C.Y. Cao, W.G. Song, J. Mater. Chem. 20 (2010) 6968–6974.
[9] A. Eyssler, A. Winkler, P. Mandaliev, P. Hug, A. Weidenkaff, D. Ferri, Appl. Catal. B: Environ. 106 (2011) 494–502.
[10] C.F. Cullis, D.L. Trimm, T.G. Nevell, J. Chem. Soc. Faraday Trans. 68 (1972) 1406–1412.
[11] F.H. Ribeiro, M. Chow, R.A. Dallabetta, J. Catal. 146 (1994) 537–544.
[12] R. Burch, F.J. Urbano, P.K. Loader, Appl. Catal. A: Gen. 123 (1995) 173–184.
[13] J.C. van Giezen, F.R. van den Berg, J.L. Kleinen, A.J. van Dillen, J.W. Geus, Catal. Today 47 (1999) 287–293.
[14] D.L. Mowery, M.S. Graboski, T.R. Ohno, R.L. McCormick, Appl. Catal. B: Environ. 21 (1999) 157–169.
[15] D. Ciuparu, N. Katsikis, L. Pfefferle, Appl. Catal. A: Gen. 216 (2001) 209–215.
[16] K. Persson, L.D. Pfefferle, W. Schwartz, A. Ersson, S.G. Jaras, Appl. Catal. B: Environ. 74 (2007) 242–250.
[17] C.B. Wang, C.M. Ho, H.K. Lin, H.C. Chiu, Fuel 81 (2002) 1883–1887.
[18] P. Hurtado, S. Ordonez, H. Sastre, F. Diez, Appl. Catal. B: Environ. 47 (2004) 85–93.
[19] K. Fujimoto, F.H. Ribeiro, M. Avalos-Borja, E. Iglesia, J. Catal. 179 (1998) 431–442.
[20] R. Burch, D.J. Crittle, M.J. Hayes, Catal. Today 47 (1999) 229–234.
[21] H. Yamamoto, H. Uchida, Catal. Today 45 (1998) 147–151.
[22] H. Yoshida, T. Nakajima, Y. Yazawa, T. Hattori, Appl. Catal. B: Environ. 71 (2007) 70–79.
[23] T.R. Baldwin, R. Burch, Appl. Catal. 66 (1990) 337–358.
[24] D.N. Gao, C.X. Zhang, S. Wang, Z.S. Yuan, S.D. Wang, Catal. Commun. 9 (2008) 2583–2587.
[25] P. Castellazzi, G. Groppi, P. Forzatti, Appl. Catal. B: Environ. 95 (2010) 303–311.
[26] R.F. Hicks, H.H. Qi, M.L. Young, R.G. Lee, J. Catal. 122 (1990) 280–294.
[27] R. Kikuchi, S. Maeda, K. Sasaki, S. Wennerstrom, K. Eguchi, Appl. Catal. A: Gen. 232 (2002) 23–28.
[28] T.Y. Chou, C.H. Leu, C.T. Yeh, Catal. Today 26 (1995) 53–58.
[29] A.F. AhlstromSilversand, C.U.I. Odenbrand, Appl. Catal. A: Gen. 153 (1997) 157–175.
[30] H. Widjaja, K. Sekizawa, K. Eguchi, H. Arai, Catal. Today 47 (1999) 95–101.
[31] L.F. Yang, C.K. Shi, X.E. He, J.X. Cai, Appl. Catal. B: Environ. 38 (2002) 117–125.
[32] L.F. Liotta, G. Deganello, J. Mol. Catal. A: Chem. 204 (2003) 763–770.
[33] M.A. Fraga, E.S. de Souza, F. Villain, L.G. Appel, Appl. Catal. A: Gen. 259 (2004) 57–63.
[34] W. Lin, Y.X. Zhu, N.Z. Wu, Y.C. Xie, I. Murwani, E. Kemnitz, Appl. Catal. B: Environ. 50 (2004) 59–66.
[35] R. Strobel, S.E. Pratsinis, A. Baiker, J. Mater. Chem. 15 (2005) 605–610.
[36] B.H. Yue, R.X. Zhou, Y.J. Wang, X.M. Zheng, Appl. Surf. Sci. 252 (2006) 5820–5828.
[37] S. Colussi, A. Trovarelli, G. Groppi, J. Llorca, Catal. Commun. 8 (2007) 1263–1266.
[38] X.H. Wang, Y. Guo, G.Z. Lu, Y. Hu, L.Z. Jiang, Y.L. Guo, Z.G. Zhang, Catal. Today 126 (2007) 369–374.
[39] P. Gelin, M. Primet, Appl. Catal. B: Environ. 39 (2002) 1–37.
[40] H. Widjaja, K. Sekizawa, K. Eguchi, H. Arai, Catal. Today 35 (1997) 197–202.
[41] V.V. Alegre, M.A.P. da Silva, M. Schmal, Catal. Commun. 7 (2006) 314–322.
[42] G. Lapisardi, L. Urfels, P. Gelin, M. Primet, A. Kaddouri, E. Garbowski, S. Toppi, E. Tena, Catal. Today 117 (2006) 564–568.
[43] A. Maione, F. Andre, P. Ruiz, Appl. Catal. B: Environ. 75 (2007) 59–70.
[44] N. Sahli, C. Petit, A.C. Roger, A. Kiennemann, S. Libs, M.M. Bettahar, Catal. Today 113 (2006) 187–193.
[45] J.J. Guo, H. Lou, H. Zhao, D.F. Chai, X.M. Zheng, Appl. Catal. A: Gen. 273 (2004) 75–82.
[46] H. Muroyama, R. Nakase, T. Matsui, K. Eguchi, Int. J. Hydrogen Energy 35 (2010) 1575–1581.
[47] K. Narui, H. Yata, K. Furuta, A. Nishida, Y. Kohtoku, T. Matsuzaki, Appl. Catal. A: Gen. 179 (1999) 165–173.
[48] J.N. Carstens, S.C. Su, A.T. Bell, J. Catal. 176 (1998) 136–142.
[49] M. Lyubovsky, L. Pfefferle, Catal. Today 47 (1999) 29–44.
[50] M. Lyubovsky, L. Pfefferle, A. Datye, J. Bravo, T. Nelson, J. Catal. 187 (1999) 275–284.
[51] P. Artizzu, E. Garbowski, M. Primet, Y. Brulle, J. Saint-Just, Catal. Today 47 (1999) 83–93.
[52] J. Requies, M.C. Alvarez-Galvan, V.L. Barrio, P.L. Arias, J.F. Cambra, M.B. Guemez, A.M. Carrera, V.A.D. la Peha O'Shea, J.L.G. Fierro, Appl. Catal. B: Environ. 79 (2008) 122–131.
[53] Y.J. Xiong, H.G. Cai, B.J. Wiley, J.G. Wang, M.J. Kim, Y.N. Xia, JACS 129 (2007) 3665–3675.
[54] Y. Ding, P.X. Gao, Z.L. Wang, JACS 126 (2004) 2066–2072.